Neuron, Volume *112*

Supplemental information

Microglial $P2Y_6$ calcium signaling promotes phagocytosis and shapes neuroimmune responses in epileptogenesis

Anthony D. Umpierre, Bohan Li, Katayoun Ayasoufi, Whitney L. Simon, Shunyi Zhao, Manling Xie, Grace Thyen, Benjamin Hur, Jiaying Zheng, Yue Liang, Dale B. Bosco, Mark A. Maynes, Zhaofa Wu, Xinzhu Yu, Jaeyun Sung, Aaron J. Johnson, Yulong Li, and Long-Jun Wu

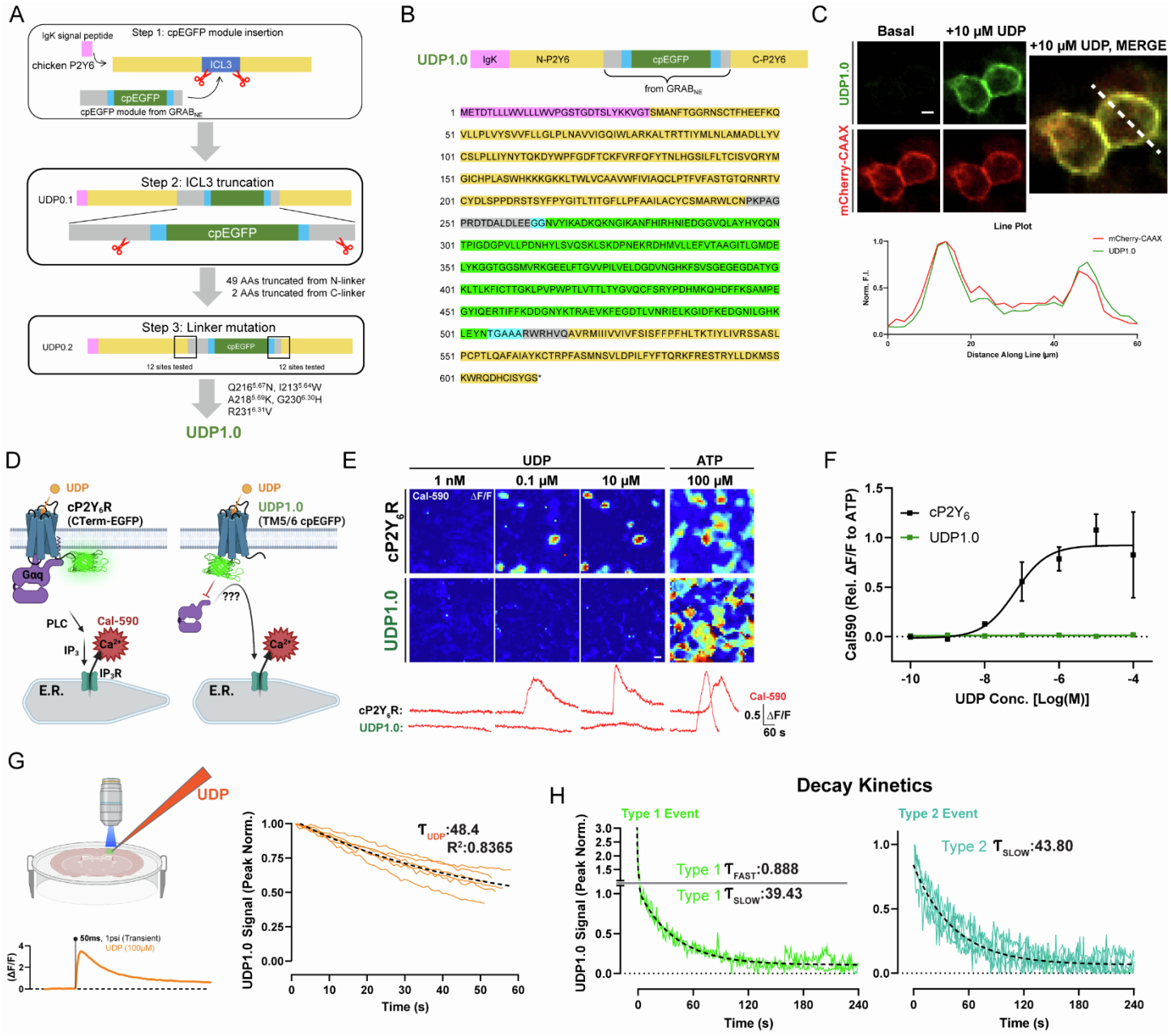

Figure S1. UDP sensor sequence, coupling, and kinetics, related to Figure 2

(A) Steps taken to optimize and refine the UDP sensor signal.

(B) Amino acid sequence of UDP1.0.

(C) Evaluation of UDP1.0 sensor trafficking to the membrane with membrane-trafficked mCherry-CAAX expression for reference.

(D) Experimental schematic: Calbryte-590 calcium imaging in response to purines using HEK cells transfected with cP2Y$_6$ or UDP1.0.

(E) Cal-590 calcium response images and corresponding ΔF/F traces from cP2Y$_6$- or UDP1.0-transfected HEK293T cells in response to purines.

(F) ATP-normalized Cal-590 fluorescent responses across a range of UDP concentrations (mean ± SEM; lines represent a non-linear fit of log (agonist) vs. 3-parameter response).

(G) Schematic of *ex vivo*, local UDP application in a UDP1.0-transfected brain slice with a representative ΔF/F response. Peak-normalized responses were used to determine the UDP1.0 single-component ⊺ decay value in response to UDP (12 trials from 3 slices and mice).

(H) One- or two-component ⊺ decay fits for Type 1 and Type 2 UDP events observed *in vivo* (⊺ value reflects 15 Type 1 and 22 Type 2 events aggregated across n=5 mice).

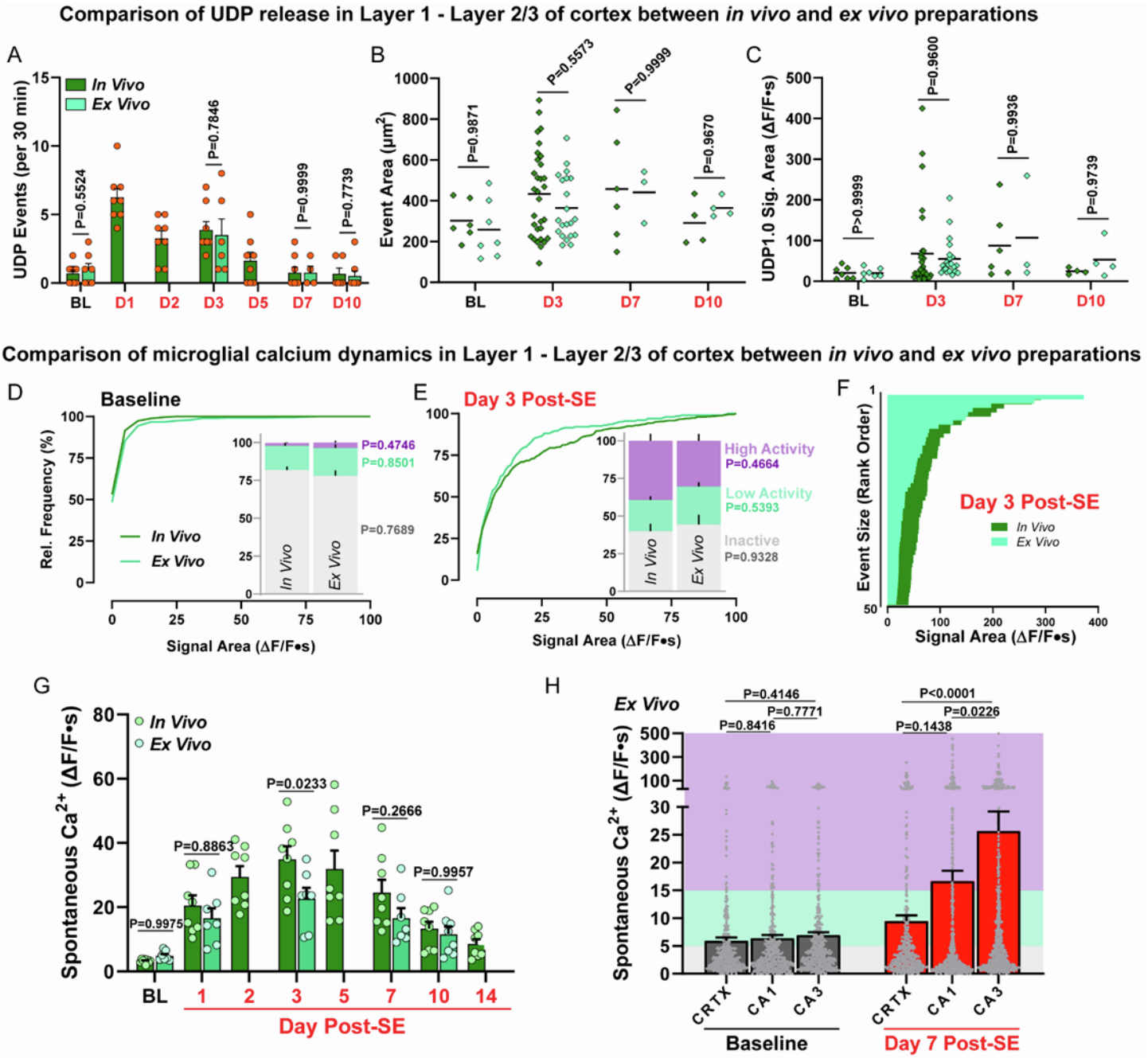

Figure S2. Comparison of UDP release dynamics and spontaneous microglial calcium activity between *ex vivo* and *in vivo* preparations in cortex, related to Figures 3 and 4

(A) Number of UDP release events reported by the UDP1.0 sensor in cortical layer 1-3 *ex vivo* (acute coronal brain slice) or *in vivo* (chronic cranial window, awake mouse) at baseline and across epileptogenesis time points. Two-way ANOVA with Sidak's post-hoc test (dot: number of UDP1.0 events detected per 30 min and field of view).

(B-C) The physical area (B: μm^2) or signal area (C: ΔF/F·s) of UDP events reported *ex vivo* or *in vivo* at baseline and across epileptogenesis time points. Two-way ANOVA with Sidak's post-hoc test (dot: a single UDP release event).

(D-E) Cumulative distribution of spontaneous calcium activity recorded from cortical microglia processes *in vivo* and *ex vivo* at baseline (D) and 3 days after KA-SE (E). Bar graphs compare the percentage of microglial ROIs which are inactive (gray bar, ΔF/F<5), display low activity (teal bar, ΔF/F=5-15), or are highly active (purple bar, ΔF/F>15). Two-way ANOVA with Sidak's post-hoc comparison between activity levels.

(F) Rank order of the largest calcium events in cortex for *in vivo* and *ex vivo* preparations 3 days after KA-SE.

(G) Microglial spontaneous calcium signaling in cortex for *in vivo* and *ex vivo* preparations. Two-way ANOVA with Sidak's post-hoc test (dot: average spontaneous calcium activity across all ROIs from a chronic window field of view (*in vivo*) or *ex vivo* slice field of view; both are 300 x 300 μm).

(H) Comparison of WT microglial spontaneous calcium activity in brain slice by region and time point. One-way ANOVA with Tukey's post-hoc test by time point (dots represent individual ROIs).

Bars represent the mean ± SEM. *In vivo* data come from n=4-5 WT mice with two regions surveyed longitudinally; *ex vivo* data come from n=4 WT mice per time point with up to two brain slices surveyed per mouse.

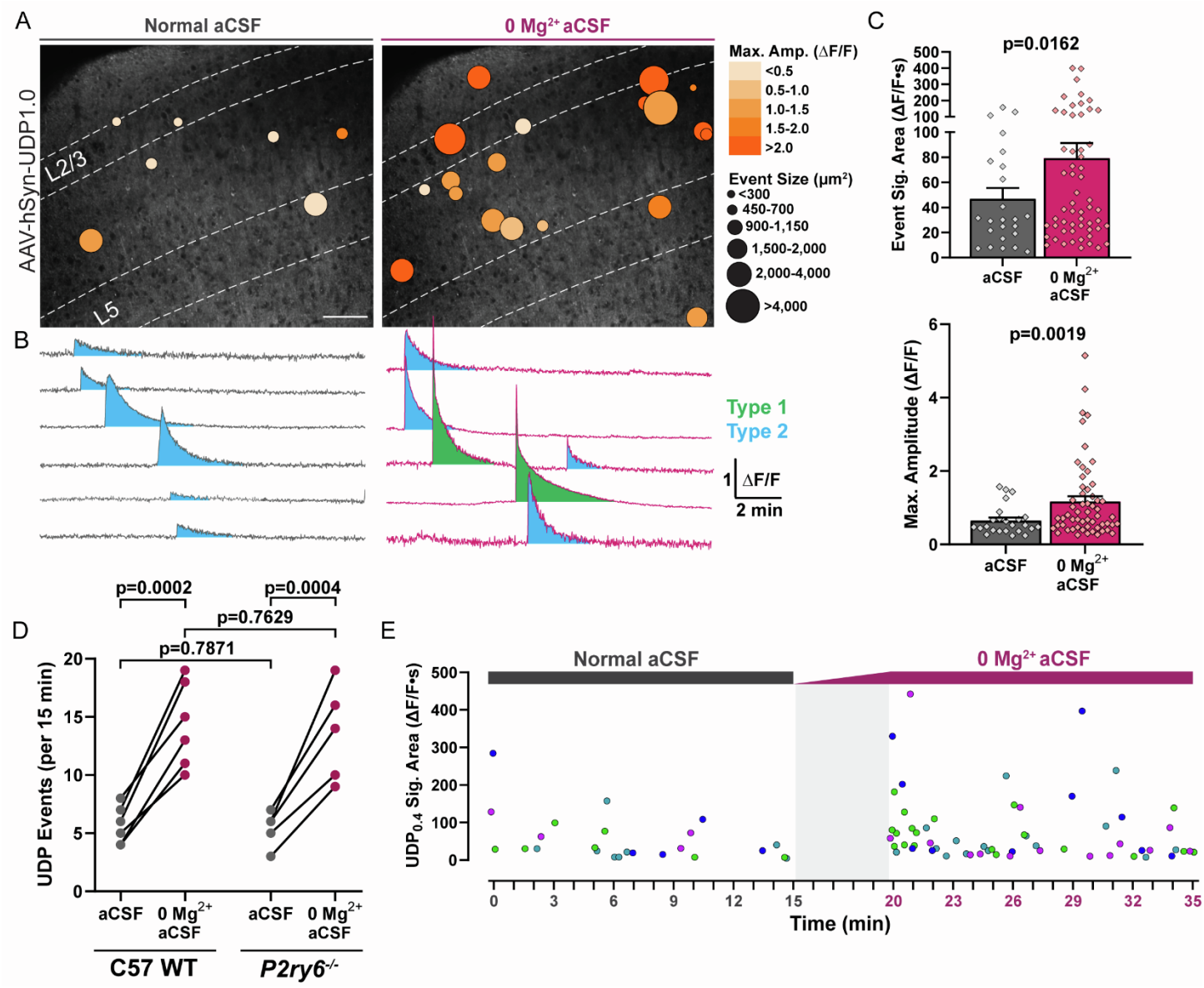

Figure S3. Enhanced UDP release during 0 Mg^{2+} hyperexcitability, related to Figure 3

(A) UDP1.0 sensor events overlaid across cortical layers during bath incubation with normal aCSF or 0 Mg^{2+} aCSF. Scale bar, 100 μm.

(B) Event traces (ΔF/F) demonstrating Type 2 events in the presence of normal aCSF, or a combination of Type 1 "sharp peak" events and Type 2 events during 0 Mg^{2+} conditions in C57 WT tissue.

(C) Comparison of UDP event signal area and maximum amplitude between normal and 0 Mg^{2+} aCSF conditions in C57 WT tissue. Student's t test (dot: one event; bar: mean ± SEM).

(D) Paired UDP event frequency under normal and 0 Mg^{2+} aCSF conditions. Within-subject aCSF vs 0 Mg^{2+} aCSF: Paired ratio t test; Between group comparisons: Student's t test (one slice per 'WT' mouse (n=4 C57 WT and n=2 *P2ry6*$^{+/+}$), one slice from n=5 *P2ry6*$^{-/-}$).

(E) Plot of UDP event signal area (ΔF/F·s) and timing over 15 min of normal aCSF incubation or 15 min of 0 Mg^{2+} aCSF incubation (gray box: 5 min solution exchange period; dot: one UDP event where color corresponds to a within-slice trial; one slice from n=4 representative WT mice).

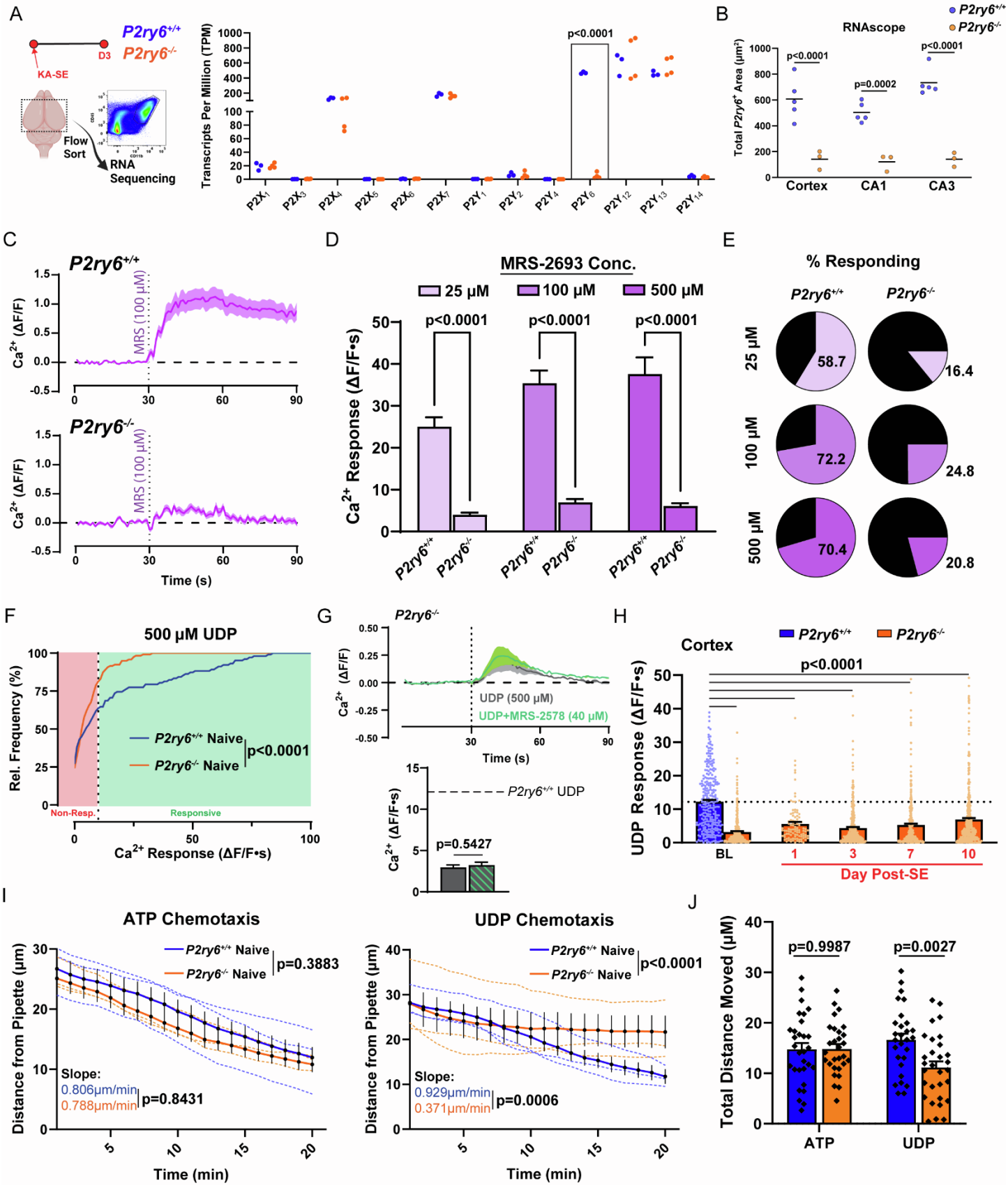

Figure S4. Functional characterization of the *P2ry6*$^{-/-}$ mouse, related to Figure 4

(A) Isolation of microglia for transcriptomic analyses 3 days after KA-SE. Confirmation of *P2ry6* transcript loss from brain microglia without changes in other P2 receptors transcripts. Two-way ANOVA with Sidak's post-hoc test (dot: one mouse/sample).

(B) RNAscope quantification of total *P2ry6* puncta hybridization area in naïve *P2ry6*$^{+/+}$ and *P2ry6*$^{-/-}$ tissue by region. Two-way ANOVA with Sidak's post-hoc test by region (dot: one imaging region per mouse; n=5 *P2ry6*$^{+/+}$ mice and n=3 *P2ry6*$^{-/-}$ mice).

(C) Representative *P2ry6*$^{+/+}$ and *P2ry6*$^{-/-}$ microglial calcium responses to MRS-2693, a high affinity $P2Y_6$ agonist, in naïve brain slice.

(D) Overall calcium responses to MRS-2693 across a concentration range. Two-Way ANOVA with Sidak's post-hoc test (all concentrations tested in 2-3 trials per slice; 1 slice from n=4 mice per genotype).

(E) Percentage of microglia responding to MRS-2693. (Average across trials; same dataset as C)

(F) Distribution of microglial calcium responses to 500 μM UDP by genotype. Welch's t test of % responding ($\Delta F/F \cdot s > 10$) by trial (2-3 trials per slice; 1 slice from n=4 mice per genotype).

(G) Representative UDP calcium response in *P2ry6*$^{-/-}$ slice in the absence or presence of bath MRS-2578, a $P2Y_6$-selective antagonist (top), and overall quantification (bottom; 1 slice from n=4 mice; unpaired t-test).

(H) UDP calcium responses in brain slice at baseline and time points following KA-SE. One-way ANOVA with Dunnett's post-hoc comparison to *P2ry6*$^{-/-}$ baseline (2 slices/mouse from n=4 mice per group and time point; dot: individual ROI).

(I) Microglial process chemotaxis towards a 1 mM ATP- or UDP-containing glass pipette. Overall effect of genotype established by Two-way ANOVA; Slope comparison established by simple linear regression (dotted lines: individual trial mean;).

(J) Total distance moved by microglial processes over a 20-min trial. Two-way ANOVA with Sidak's post-hoc test (dot: individual process; survey of 28-30 processes from 3 separate slices and animals per group).

Bar graphs and shaded line graphs both display the mean ± SEM.

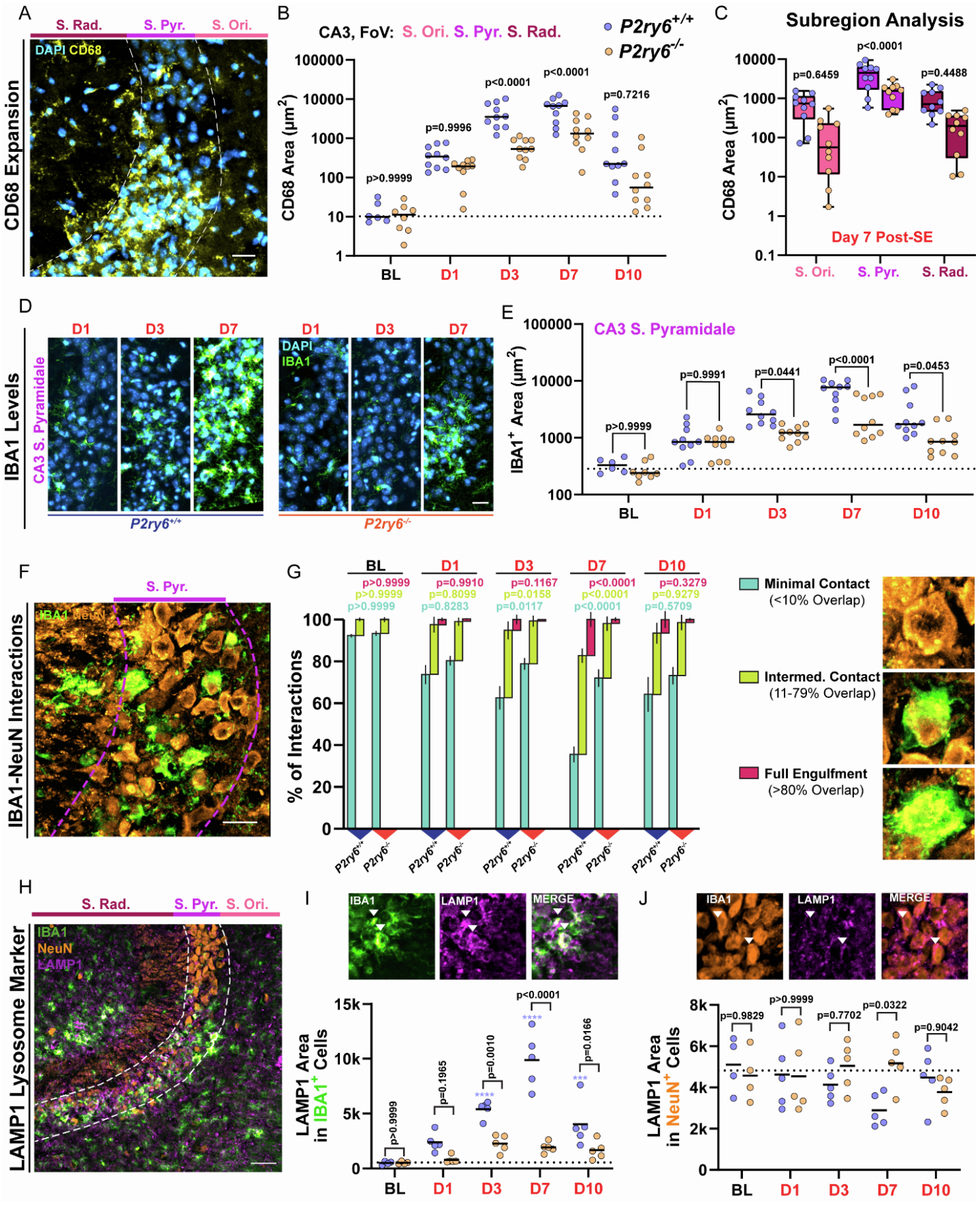

Figure S5. Evolution of phagocytic interactions in CA3, related to Figure 5

(A) Image of CD68 staining in CA3 from a day 7 post-SE WT mouse. Scale bar, 20µm.

(B) Quantification of CD68 area over time from the entire CA3 field of view. Two-way ANOVA with Sidak's post-hoc test.

(C) CD68 staining between genotypes day 7 post-SE by CA3 subregion. One-way ANOVA with Sidak's post-hoc test.

(D) Representative images of IBA1 (green) in the CA3 pyramidal band during early epileptogenesis. Scale bar, 20μm.

(E) Quantification of IBA1 area over time in the CA3 pyramidal band. Two-way ANOVA with Sidak's post-hoc test.

(F) IBA1 and NeuN cell interactions day 7 post-SE in the CA3 pyramidal layer of a WT mouse. Scale bar, 20μm.

(G) Percentage of CA3 NeuN neurons having minimal/no contact with IBA1 cells, intermediate contact, or reaching full engulfment criteria across time (examples on the right). Two-way ANOVA with Sidak's post-hoc test by interaction type.

(H) Staining for LAMP1, IBA1, and NeuN in the CA3 region 7 days post-SE (image from a WT mouse). Scale bar, 50μm.

(I) (Top) Example of LAMP1 lysosome regions overlapping with $IBA1^+$ cell volume. (Bottom) Quantification of LAMP1 area colocalized with IBA1 over time in the CA3 region. Two-way ANOVA with Sidak's post-hoc test between genotypes (black bars with exact p-values). Two-way ANOVA with Dunnett's post-hoc comparison between WT baseline and post-SE time points (blue asterisks).

(J) (Top) Example of LAMP1 lysosome regions overlapping with $NeuN^+$ cell volume. (Bottom) Quantification of LAMP1 area colocalized with NeuN over time in the CA3 region. Two-way ANOVA with Sidak's post-hoc test between genotypes.

Bars represent the mean ± SEM. Dots represent one of two hippocampi surveyed per mouse. n=3-5 mice per group.

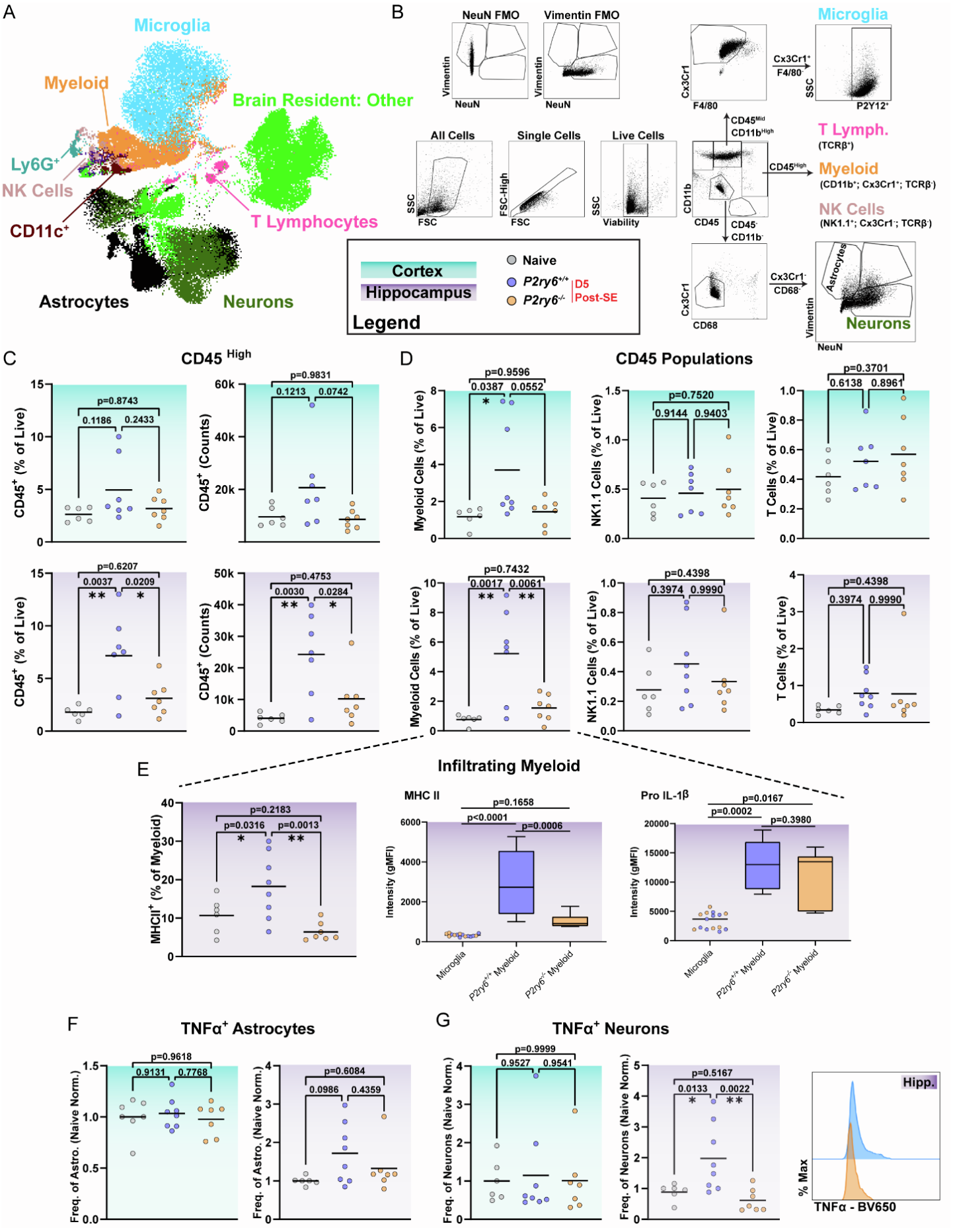
A
Microglia
Myeloid
Brain Resident: Other
Ly6G+
NK Cells
CD11c+
T Lymphocytes
Astrocytes
Neurons
B
NeuN FMO
Vimentin FMO
Vimentin
NeuN
Microglia
Cx3Cr1
F4/80
Cx3Cr1+ F4/80-
SSC
P2Y12+
All Cells
Single Cells
Live Cells
SSC
FSC
FSC-High
Viability
CD45Mid CD11bHigh
CD11b
CD45
CD45High
CD45- CD11b-
T Lymph.
(TCRβ+)
Myeloid
(CD11b+; Cx3Cr1+; TCRβ-)
NK Cells
(NK1.1+; Cx3Cr1-; TCRβ-)
Cx3Cr1- CD68-
CD68
Astrocytes
Neurons
Cortex
Hippocampus
Legend
Naive
P2ry6+/+ D5
P2ry6-/- Post-SE
C
CD45 High
CD45+ (% of Live)
CD45+ (Counts)
p=0.8743
0.1186
0.2433
p=0.9831
0.1213
0.0742
p=0.6207
0.0037
0.0209
p=0.4753
0.0030
0.0284
D
CD45 Populations
Myeloid Cells (% of Live)
NK1.1 Cells (% of Live)
T Cells (% of Live)
p=0.9596
0.0387
0.0552
p=0.7520
0.9144
0.9403
p=0.3701
0.6138
0.8961
p=0.7432
0.0017
0.0061
p=0.4398
0.3974
0.9990
E
Infiltrating Myeloid
MHCII+ (% of Myeloid)
p=0.2183
p=0.0316
p=0.0013
MHC II
Intensity (gMFI)
p=0.1658
p<0.0001
p=0.0006
Pro IL-1β
p=0.0167
p=0.0002
p=0.3980
Microglia
P2ry6+/+ Myeloid
P2ry6-/- Myeloid
F
TNFα+ Astrocytes
Freq. of Astro. (Naive Norm.)
p=0.9618
0.9131
0.7768
p=0.6084
0.0986
0.4359
G
TNFα+ Neurons
Freq. of Neurons (Naive Norm.)
p=0.9999
0.9527
0.9541
p=0.5167
0.0133
0.0022
Hipp.
% Max
TNFα - BV650

Figure S6. Greater pro-inflammatory myeloid infiltration occurs in *P2ry6*$^{+/+}$ hippocampus, related to Figure 7

(A) UMAP of resident and infiltrating cell populations built off FSC, SSC, all surface markers and cytokines (see STAR Methods).

(B) Gating strategy to separate microglia, infiltrating immune populations, and other resident brain cells.

(C) The number (counts) and frequency (% live) of CD45^{+} immune cell populations between regions and genotypes.

(D) Further evaluation of infiltrating CD45^{High} cells based upon markers defining myeloid, NK, or T lymphocyte sub-populations.

(E) Differences in MHCII expression frequency and intensity (gMFI) between infiltrating myeloid population in *P2ry6*$^{+/+}$ and *P2ry6*$^{-/-}$ hippocampus and in reference to resident microglia. Pro IL-1β expression in infiltrating myeloid cells relative to resident microglia.

(F) Evaluation of TNF-α expression frequency by vimentin^{+} astrocytes in cortex and hippocampus.

(G) Expression of TNF-α in NeuN^{+} neurons, including frequency and mode-normalized representative histograms.

Data come from n=6 naïve mice (4 WT, 2 KO), n=8 *P2ry6*$^{+/+}$ mice and n=7 *P2ry6*$^{-/-}$ mice from two independent cohorts. Scatter plots: dot represents one mouse, line at the mean. Box and whisker plots display mean, interquartile range, and min to max. Significance testing utilized a One-way ANOVA with Tukey's post-hoc test.

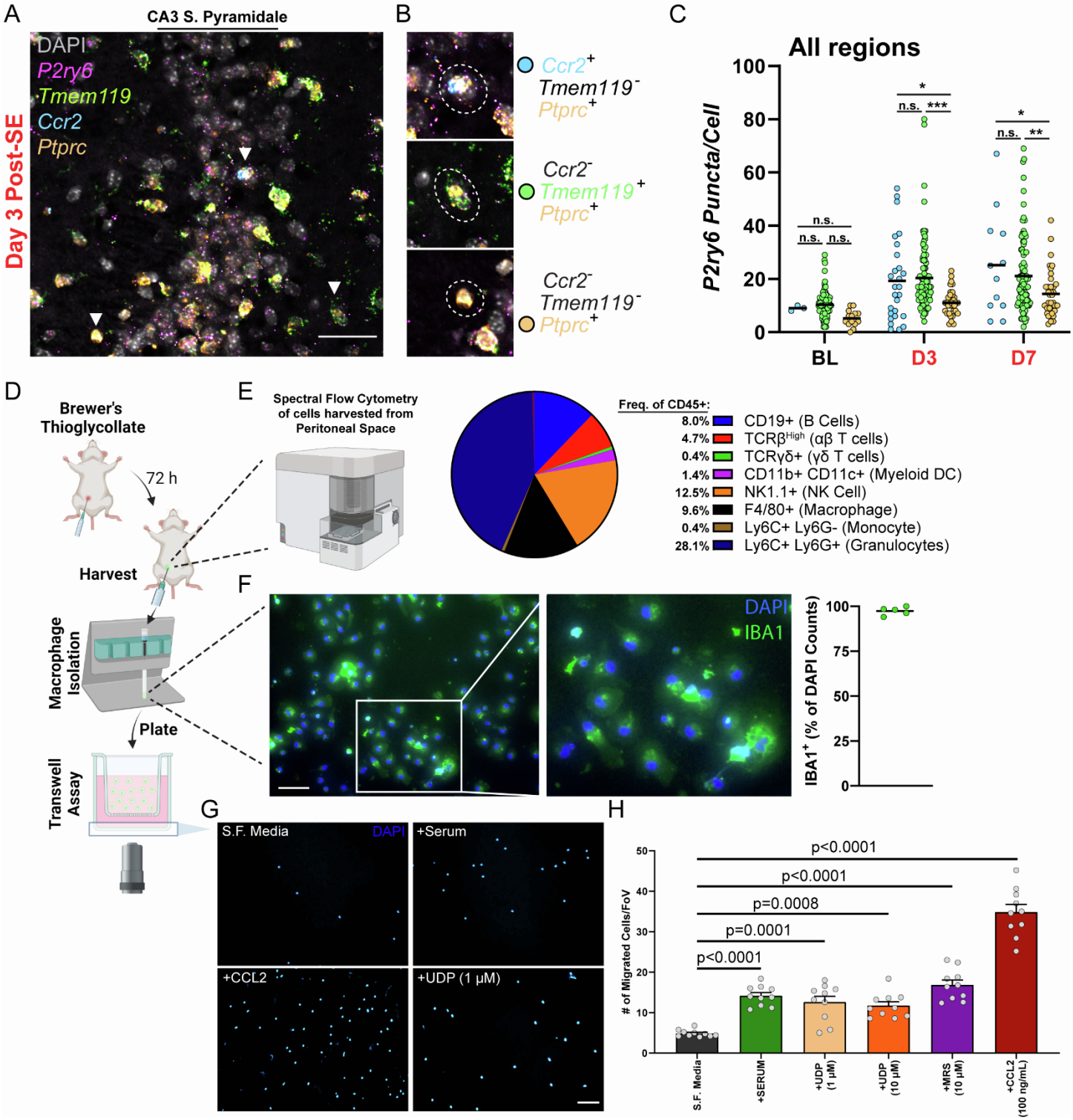

Figure S7. Myeloid cell *P2ry6* transcription and UDP-based cell migration/invasion, related to Figure 7

(A) RNAscope imaging of the CA3 region 3 days after KA-SE with DAPI staining and probes hybridized against *P2ry6*, *TMEM119, Ccr2,* and *Ptprc* (the transcript encoding CD45 protein). Scale bar, 50 μm.

(B) Example *Ccr2*$^+$ immune cell (*Ptprc*$^+$), microglial cell (*Tmem119*$^+$*; Ccr2*$^-$; *Ptprc*$^+$), and undefined immune cell (*Ptprc*$^+$). Cells in (B) are depicted by arrows in (A).

(C) Quantification of *P2ry6* puncta within a 2 μm expanded radius around DAPI nuclei, categorized and color coded in (B). Dots represent the puncta for a single cell, aggregated across all imaging regions (Cortex, CA3, and CA1) by time point. One-way ANOVA with Tukey's post-hoc test per each time point (n.s.: not significant; n=5 naïve C57 WT mice and n=4 C57 WT mice for day 3 and day 7 post-SE).

(D) Schematic depiction of transwell migration assay process.

(E) Characterization of the CD45$^+$ immune cell populations obtained from the intraperitoneal space after Brewer's Thioglycolate challenge.

(F) Evaluation of IBA1$^+$ nucleated cell purity following macrophage isolation (see STAR METHODS), with quantification of IBA1$^+$ cells from the DAPI nucleated population (5 replicate wells; dot: average of 3 fields of view per well). Scale bar, 25 μm.

(G) Representative images of DAPI nucleated cells on the bottom of a well after a 24h transwell migration assay. Cells plated on the transwell mesh (8 μm pore; 6.5 mm diameter) were obtained following the use of a macrophage isolation kit (as in F). Scale bar, 100 μm.

(H) Quantification of DAPI nucleated cells on the bottom of the transwell plate by chemoattractant/condition. One-way ANOVA with Dunnett's post-hoc comparison to serum-free (S.F.) Media (dots represent the average cell number from imaging 5 randomized fields of view per well; 10 wells per condition).

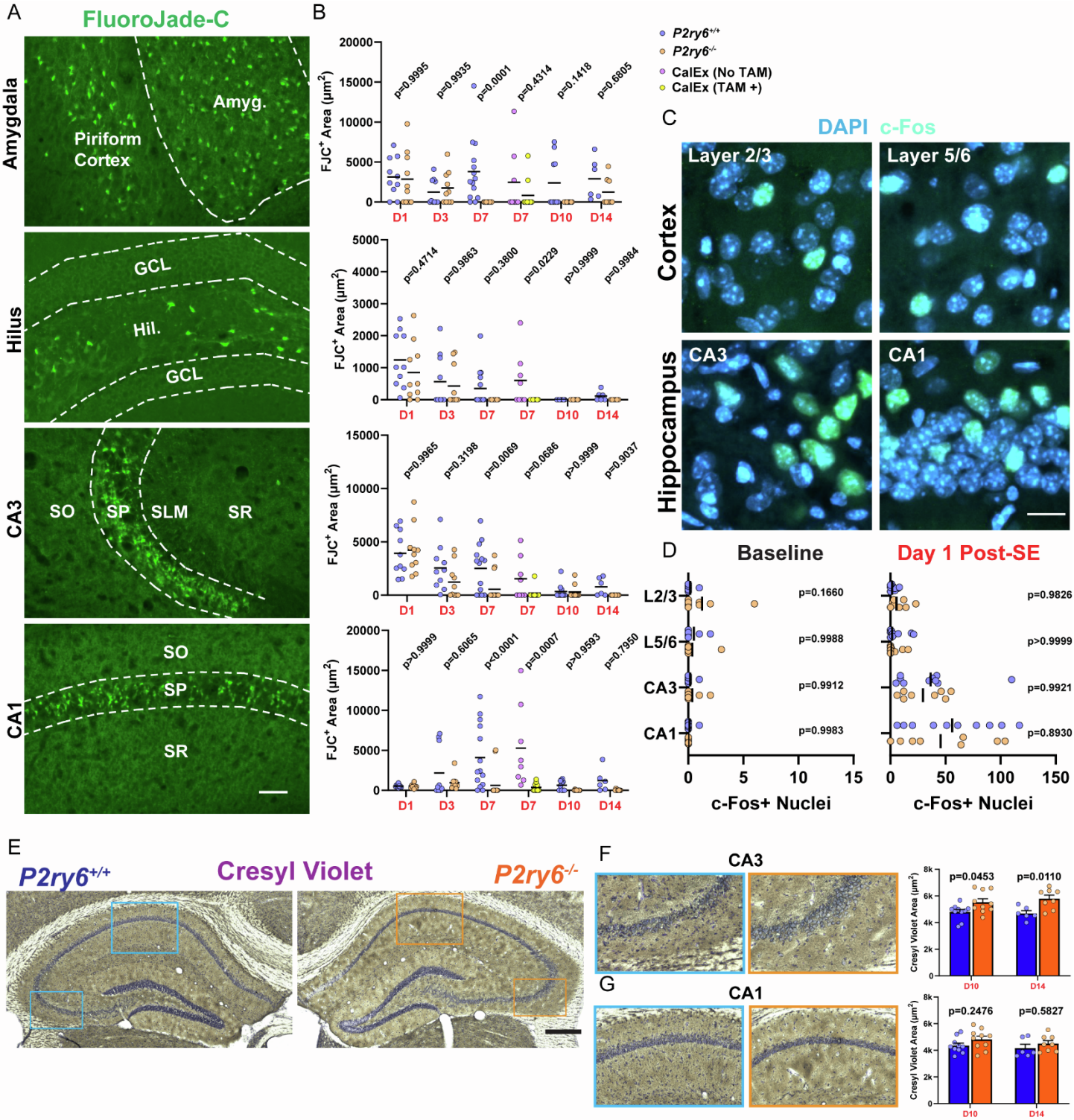

Figure S8. Comparison of neuropathology and seizure damage between genotypes, related to Figure 8

(A) Representative images of FluoroJade-C (FJC) staining one day after KA-SE in the amygdala, hilus, CA3, and CA1 regions. Scale bar, 50 μm. (GCL:Granule Cell Layer).

(B) Quantification of FJC-positive cell area by region between *P2ry6*$^{+/+}$ and *P2ry6*$^{-/-}$ mouse tissue (over time) or CalEx tissue and its tamoxifen-restricted control (day 7 post-SE). Two-Way ANOVA with Sidak's post-hoc comparison (dot: one region; bilateral survey from n=3-9 mice per group).

(C) Examples of DAPI and c-Fos staining one day after KA-SE. Scale bar, 15 μm.

(D) Quantification of c-Fos positive nuclei between genotypes at baseline and one-day after KA-SE. Two-way ANOVA with Sidak's post-hoc test by region (dot: one region; bilateral survey from n=4-5 mice per group).

(E) Representative hippocampi stained with Cresyl Violate acetate 14 days after KA-SE. Scale bar, 500 μm.

(F, G) Enlarged images of the CA3 (F) and CA1 (G) regions with corresponding quantification of Cresyl Violet area within the pyramidal band. Two-way ANOVA with Sidak's post-hoc test (dot: one region; bilateral survey from n=3-5 mice per group).